JOURNAL OF SOLID STATE CHEMISTRY **141,** 262–269 (1998)
ARTICLE NO. SC987989

An Investigation of the Magnetic Properties of $Sm_{1-x}TiO_3$ for $x = 0.03$, 0.05, and 0.10: Magnetic Structure Determination of $Sm_{0.97}TiO_3$ by Short-Wavelength Neutron Diffraction on Single Crystals

G. Amow,* J. E. Greedan,*,[1] and C. Ritter†

*Department of Chemistry and the Brockhouse Institute for Materials Research, McMaster University, Hamilton, Ontario L8S 4M1, Canada; and †Institut Max von Laue-Paul Langevin, Ave. des Martyrs, B.P. 156, F-38042 Grenoble Cedex 9, France

Received April 16, 1998; in revised form July 27, 1998; accepted August 3, 1998

Single crystals of $Sm_{0.97}TiO_3$ have been prepared and their magnetic properties have been investigated. Dc magnetic susceptibility measurements indicate paramagnetic Curie–Weiss behavior above 100 K whereas two magnetic transitions are observed at $T_N \sim 52$ K and $T_N \sim 40$ K. Similar observations for antiferromagnetic behavior have been made for the $x = 0.05$ compound with $T_N \sim 40$ K whereas for the $x = 0.10$ compound this behavior vanishes. The magnetic structure determination of the $x = 0.03$ compound has been accomplished by using low-temperature single-crystal neutron diffraction. The room temperature crystal structure is a distorted orthorhombic perovskite structure belonging to *Pnma*, which is preserved down to 15 K. The magnetic structure is found to be consistent with a G_xG_y moment configuration on the Ti(III) sublattice and a C_z moment configuration on the Sm(III) sublattice. The magnetic moments are estimated to be 0.72(1) and 0.43(1) μ_B on the Ti(III) and Sm(III) sublattices, respectively. The orientations of the moments were found to be 7(3)° to the x-axis for Ti(III) and 2(2)° to the z-axis for Sm(III).

INTRODUCTION

As part of a greater body of research involving the vacancy-doped rare earth titanate system $R_{1-x}TiO_3$ (R = La, Nd, and Sm), we are interested in the investigation of the magnetic properties of these compounds. In general, the vacancy-doped rare earth titanates as well as the alkaline earth doped systems $R_{1-x}A_xTiO_3$ are of interest as in these cases electron correlation effects strongly influence the physical properties of member compounds. Consequently, they allow systematic studies of the physical properties as a function of band filling (1–4).

The magnetic properties as well as the magnetic structure determination of the samarium titanate $SmTiO_3$ are of special interest in light of the known behavior of the $RTiO_3$ series of compounds (R = La–Gd, Y). A remarkable variation in the magnetic properties as a function of decreasing rare earth radius exists, ranging from antiferromagnetic Ti–Ti coupling for R = La, Ce, Pr, and Nd to ferromagnetic Ti–Ti coupling for R = Gd–Lu, Y (5–8). In spite of the interesting position of Sm in the series, evidence for any type of magnetic ordering for the R = Sm compound had remained elusive (9). Until recently, however, there has been one published report indicating that $SmTiO_3$ undergoes some type of ordering phenomenon at ~ 50 K. Despite this, a detailed investigation into the magnetic properties as well as the magnetic structure determination for this compound has not been performed (10).

Unlike the magnetic structure determinations for the R = La, Ce, Pr, and Nd titanates, for which low-temperature powder neutron diffraction was used, the case of samarium titanate presents an interesting challenge due to the high absorption cross section of Sm at conventional thermal neutron wavelengths >1 Å (~ 5760 barns). It is known that this value decreases sharply to ~ 500 barns at a wavelength of 0.5 Å, thus, in principle, making this problem more tractable if hot source neutrons are available (11). The neutron source at the Institut Laue-Langevin (ILL), Grenoble, France, is ideally suited for this study as it provides accessibility to very short wavelengths coupled with high flux. Furthermore, by utilizing low-temperature single-crystal neutron diffraction, it is possible for the first time to determine the magnetic structure of a rare earth titanate unambiguously. As mentioned previously, the magnetic structure determinations of the rare earth titanates to date have been principally carried out with low-temperature powder neutron diffraction. While this method has had some success, the magnetic structures remain somewhat

[1]To whom correspondence should be addressed. E-mail: greedan@mcmail.cis.mcmaster.ca.

0022-4596/98 $25.00

ambiguous due to the inability of the method to resolve overlapping magnetic reflections. We present in this report an investigation of the magnetic properties of $SmTiO_3$ as well as its magnetic structure determination by low-temperature single-crystal neutron diffraction, the first such study to be carried out for any of the rare earth titanates.

EXPERIMENTAL

Sample Preparation

The nominal $x = 0.00$ composition was prepared by mixing stoichiometric amounts of predried Sm_2O_3 (5.0000 g, Rhone Poulenc, 99.99%), TiO_2 (0.9941 g, Cerac, 99.9%), and $TiO_{1.046}$ (1.0498 g, Cerac, 99.9%) in acetone. In the case of the $x = 0.05$ and $x = 0.10$ compositions, Ti_2O_3 (Cerac, 99.9%) was used. For each sample the reagents were pressed into 1/2-in. pellets and sealed in a molybdenum crucible. The sealed crucible was then placed into an rf furnace and was fired several times at $\sim$1400°C under vacuum (10^{-6} Torr) for $\sim$12 h each time to achieve phase purity. The pellets were reground and pressed between each firing. The polycrystalline products obtained were black.

Single crystals for the nominal $x = 0.00$ phase were obtained by firing the polycrystalline sample to just above its melting point ($\sim$1800°C) and then quenching to room temperature. The crystals were obtained as shiny black blocks with defined faces having an average dimension of $\sim 1.5\text{ mm} \times 1.5\text{ mm} \times 1\text{ mm}$.

X-Ray Powder Diffraction

Phase purity determination was carried out with a Guinier–Haag camera (IRDAB Model XDC700) with Cu$K\alpha_1$ radiation and silicon as an internal standard. A KEJ Instruments line scanner (Model LS20) was used to measure the positions and intensities of the diffraction lines. Unit cell constants were refined with the least-squares program LSUDF.

Thermal Gravimetric Analysis

The oxygen content of the sample was determined with a Netzch STA thermal analyzer in flowing air at 1000°C.

Magnetic Susceptibility

Dc magnetic susceptibility measurements were carried out with a Quantum Design SQUID magnetometer in the temperature range of 5–300 K using an applied field of 100 Oe.

Powder Neutron Diffraction

Data were collected at 298 and 1.5 K on the D1B powder diffractometer at the ILL using a wavelength of 2.52 Å over the 2θ range 10–90°. The sample was diluted with aluminum powder to minimize the strong absorption presented by samarium.

Single-Crystal X-Ray Diffraction

Data were collected at room temperature with a Siemens P3 four-circle diffractometer using Ag$K\alpha$ radiation ($\lambda = 0.56086$ Å). The data were corrected for absorption effects by the semiempirical ψ-scan method. For further details of the data collection, see Table 2.

Single-Crystal Neutron Diffraction

Neutron data were collected with the D9 four-circle single-crystal diffractometer at the ILL equipped with a two-dimensional position-sensitive detector. A wavelength of $\lambda = 0.4710$ Å was obtained by reflection from a Cu(220) single-crystal monochromator. To follow the thermal development of the magnetic reflections, measurements were made at room temperature and at 15 K with the use of a Displex cryostat. Several low-angle magnetic reflections were scanned for approximately 6 h each using an ω scan. A full data set for the purpose of structural refinement at 15 K was also collected. The integrated intensities were obtained by RACER (12). No absorption corrections were made to the data. Structural refinement was carried out with SHELXTL-93 (13) and details of the refinement can be found in Table 2.

RESULTS AND DISCUSSION

Structural Characterization

The room temperature crystal structure of $SmTiO_3$ has been reported previously (14). The structure is an orthorhombically distorted perovskite type belonging to the space group *Pnma*, typical for the $RTiO_3$ series, and is found to be preserved for the $x = 0.03$ to $x = 0.10$ compositions (see Fig. 1). The unit cell constants derived from the Guinier–Haag data for all three compositions are summarized in Table 1. The unit cell volume for the sample used in the present study is marginally larger (within 0.5%) than that reported by Maclean *et al.* (13), suggesting that the composition is closer to the nominal composition of $SmTiO_3$. The single-crystal X-Ray data collected at room temperature refined smoothly in *Pnma* to the values shown in Table 2. In addition, the samarium content was refined and in this manner the composition was determined to be $Sm_{0.97}TiO_3$. This result is consistent with the experimental weight gain of 3.08% obtained by TGA, which compares favorably with the expected gain of 3.01% for this stoichiometry. The refined positional and thermal parameters as well as selected geometrical parameters can be found in Tables 3–5.

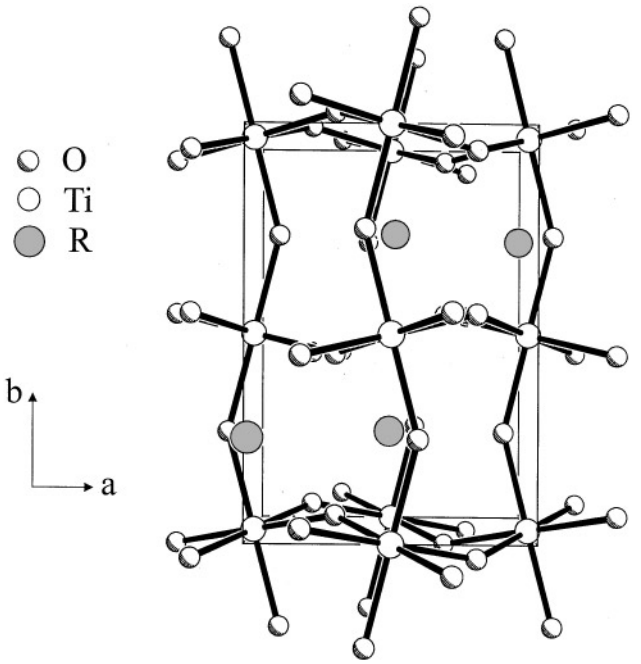

FIG. 1. Crystal structure of $R\mathrm{TiO_3}$ (R = rare earth).

With regard to the crystal structure at 15 K, although no absorption corrections were made to the neutron data, the refinement proceeded smoothly in *Pnma*, indicating no change in the crystal structure at this temperature (see Table 2). This observation is further supported qualitatively by the neutron powder profiles obtained, which showed very little change between 298 and 1.5 K. During the refinement process a strong correlation was observed between the site occupancy of Sm and its temperature factor. Consequently the Sm temperature factor was refined to an initial isotropic value and was subsequently constrained throughout the refinement while the temperature factors of the remaining atoms were refined anisotropically. In addition, 22 weak reflections were present in the data set that violated *Pnma* symmetry. However, these are likely to be artifacts of multiple scattering processes and were ignored in the refinement. The positional and thermal parameters as well as selected geometrical parameters can be found in Tables 3–5. Finally, a comparison of the cell volumes as well as the bond distances at 298 and 15 K (Table 5) shows the expected decreases in values as the temperature is lowered.

TABLE 1

Sample	a (Å)	b (Å)	c (Å)	V (Å^3)
$SmTiO_3$[a]	5.660(2)	7.722(4)	5.454(2)	238.4(2)
$Sm_{0.97}TiO_3$	5.6654(3)	7.7298(4)	5.4623(3)	239.21(2)
$Sm_{0.95}TiO_3$[b]	5.6154(6)	7.74166(6)	5.4542(4)	237.11(3)
$Sm_{0.90}TiO_3$[b]	5.5774(7)	7.7450(7)	5.4464(6)	235.27(3)

[a] From single-crystal work by Maclean *et al.* (5).
[b] Nominal composition.

TABLE 2

Crystal Data and Refinement Parameters for $SmTiO_3$ Obtained from X-Ray and Neutron Data Collected at 298 and 15 K, Respectively

	X-ray data	Neutron data
Color	Black	Black
Crystal size (mm)	0.1 (sphere)	$2.5 \times 2.5 \times 1.5$
Crystal system	Orthorhombic	Orthorhombic
Space group	*Pnma*	*Pnma*
Unit cell dimensions (Å)	$a = 5.6528(11)$	$a = 5.5902(11)$
	$b = 7.7082(15)$	$b = 7.6467(15)$
	$c = 5.4478(11)$	$c = 5.4329(11)$
Volume (Å^3)	237.3765(37)	231.8532(37)
Z	4	4
Formula weight	246.26	246.26
Density (calc) (g/cm^3)	6.890	6.890
Wavelength	Ag$K\alpha$ ($\lambda = 0.56086$ Å)	$\lambda = 0.4710$ Å
T (K)	298	15
2θ range (deg)	3.5–90.25	5–35.93
Scan type	ω–2θ	ω–2θ
Linear absorption coefficient (mm^{-1})	14.63	—
Absorption correction	ψ-scan	None
$F(000)$	432.0	432.0
Index ranges	$-1 \le h \le 14$,	$0 \le h \le 7$,
	$-1 \le k \le 19$,	$0 \le k \le 10$,
	$-1 \le l \le 13$	$0 \le l \le 7$
Standard reflections	One every 97 reflections	One every 52 reflections
Number of reflections collected	2986	664
Number of independent reflections	2079	289
Restraints/parameters	0/29	1/25
Rms residual electron density, ρ_{rms} (e/Å^3)	1.13	0.22
wR_2[a]	15.20	14.20
R_1[a]	6.21	5.30

[a] $wR_2 = [\sum w(F_o^2 - F_c^2)/\sum w(F_o^2)^2]^{1/2}$; $R_1 = (\sum ||F_o| - |F_c||)/\sum |F_o|$.

Magnetic Properties

The magnetic susceptibility behavior over the temperature range 5–298 K for $Sm_{0.97}TiO_3$ can be seen in Fig. 2. Above 100 K it was found that Curie–Weiss paramagnetism exists and the data could be fitted to

$$\chi = \frac{C}{(T - \Theta)},$$

where C is the Curie constant and Θ is the Weiss constant. The data were corrected for core diamagnetism, and experimentally determined values were found to be $C = 1.07(1)$ cm^3 mol K^{-1} and $\Theta = -229(5)$ K. Clearly apparent

TABLE 3
Refined Positional and Thermal Parameters at 298 and 15 K

	298 K[a]	15 K[b]
Sm		
x	0.06472(4)	0.06632(39)
y	0.25	0.25
z	0.98448(4)	0.98590(38)
U_{eq}(Å^2)	0.01110(6)	0.00251(0)
Ti		
x	0.5	0.5
y	0.5	0.5
z	0	0
U_{eq}(Å^2)	0.00986(13)	0.00921(67)
O1		
x	0.47342(63)	0.47588(34)
y	0.25	0.25
z	0.10239(72)	0.10189(36)
U_{eq}(Å^2)	0.01324(30)	0.01113(45)
O2		
x	0.30387(41)	0.30396(22)
y	0.05175(31)	0.05174(18)
z	0.69654(44)	0.69786(22)
U_{eq}(Å^2)	0.01302(40)	0.01125(45)

[a]X-Ray data.
[b]Neutron data.

TABLE 5
Selected Bond Distances (Å) and Bond Angles (Deg)

		298 K[a]	15 K[b]
Sm–O1	×1	3.404(4)	3.360(3)
Sm–O1	×1	3.239(4)	3.228(3)
Sm–O1	×1	2.398(4)	2.374(3)
Sm–O1	×1	2.309(4)	2.292(3)
Sm–O2	×2	3.5737(24)	3.5427(21)
Sm–O2	×2	2.7012(24)	2.6779(18)
Sm–O2	×2	2.5736(24)	2.5503(22)
Sm–O2	×2	2.3414(24)	2.3330(21)
Ti–O1	×2	2.0630(24)	2.0483(13)
Ti–O2	×2	2.0301(24)	2.0108(12)
Ti–O2	×2	2.0118(12)	1.9945(7)
O1–Ti–O1		180	180
O2–Ti–O2		90.34(9)	90.74(5)
		89.66(9)	89.26(5)
O1–Ti–O2		88.80(12)	89.08(7)
		91.20(12)	90.92(7)
		89.82(13)	90.02(7)
		90.18(13)	89.98(7)
Ti–O1–Ti		146.63(21)	146.86(11)
Ti–O2–Ti		147.07(13)	147.26(7)

[a]X-ray data.
[b]Neutron data.

is the sharp transition at ~ 52 K, indicating the onset of antiferromagnetic behavior. At ~ 40 K there is a smaller feature which is likely the result of a spin-reordering process on the magnetic sublattices. Furthermore, the divergence between the zero-field-cooled (ZFC) and field-cooled (FC) data indicates the presence of a weak ferromagnetic moment which can be ascribed to moment canting on the sublattices.

It should be pointed out that the susceptibility behavior in Fig. 2 bears a strong resemblance to that observed for $NdTiO_3$ (8). It has been shown that a likely model for the magnetic structure for this compound (as well as $PrTiO_3$ and $CeTiO_3$) has a *C*-type spin configuration on the Nd(III) sublattice and a *G*-type spin configuration on the Ti(III) sublattice (6, 8).

The magnetic reflections which arise as a consequence of *G*-type and *C*-type ordering belong to $h + 1 = \text{odd}, k = \text{odd}$

TABLE 4
Anisotropic Thermal Parameters (Å) for $SmTiO_3$ at 298 and 15 K

298 K[a]	U_{11}	U_{22}	U_{33}	U_{23}	U_{13}	U_{12}
Sm1	0.01071(8)	0.01159(8)	0.01100(8)	0	− 0.00081(4)	0
Ti	0.00961(21)	0.01008(21)	0.00990(21)	0.00020(13)	− 0.00002(13)	− 0.00010(14)
O1	0.01162(60)	0.01566(70)	0.01244(61)	0.00082(51)	− 0.00237(50)	− 0.00181(55)
O2	0.01252(90)	0.01185(83)	0.01470(99)	0	− 0.00082(77)	0
15 K[b]	U_{11}	U_{22}	U_{33}	U_{23}	U_{13}	U_{12}
Sm[c]	—	—	—	—	—	—
Ti	0.00935(130)	0.01113(153)	0.00719(128)	0.00007(107)	0.00028(90)	− 0.00027(115)
O1	0.01039(71)	0.01301(70)	0.01041(79)	0.00040(42)	− 0.00137(48)	− 0.00091(43)
O2	0.01030(86)	0.01123(90)	0.01191(91)	0	− 0.00026(65)	0

[a]X-ray data.
[b]Neutron data.
[c]The Sm temperature factor was refined isotropically.

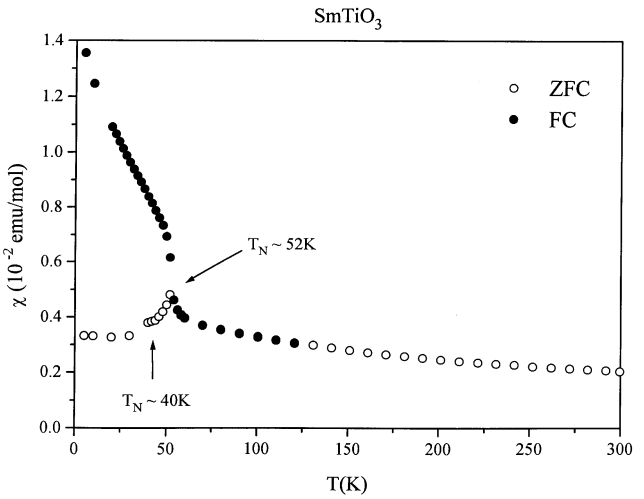

FIG. 2. Magnetic susceptibility (χ) vs T for $SmTiO_3$.

and $h + 1 =$ odd, $k =$ even, respectively, in the *Pnma* setting. Thus, in a typical low-temperature powder neutron diffraction experiment involving the rare earth titanates, the proper indexing of the magnetic reflections can give information about the arrangement of spins, i.e., *G*-type or *C*-type. However, since it is not possible to resolve the intensities of overlapping magnetic reflections, for example the *G*-type (110, 011) reflections, it becomes difficult to determine the precise orientation of the spins relative to the principal axes of the unit cell. This point is compellingly exemplified by the magnetic structure determination of $CeTiO_3$, for which three models were found to be possible, each consistent with the intensity data obtained (6). By performing a single-crystal diffraction experiment, it should, in principle, be possible to remove any ambiguity in obtaining the correct description for the orientation of spins as it allows for the resolution and independent measurement of magnetic peak intensities.

Initially, the magnetic structure for $Sm_{0.97}TiO_3$ was assumed to be the same as for the La–Nd titanates. Experience has shown that the strongest reflections are (110) and (011) for *G*-type ordering and (021) and (120) for *C*-type ordering, where the latter three reflections are forbidden in *Pnma*. Consequently, the thermal development of the (110), (011), (120), and (021) reflections was followed by measuring their intensities at 298 and 15 K. Preliminary scans of these reflections at 15 K, lasting 30 min each, revealed negligible intensity in each case. However, with substantially longer counting times (6 h for each reflection), significant intensities were recorded which were observed to have decreased drastically at room temperature (see Figs. 4 and 5). The results

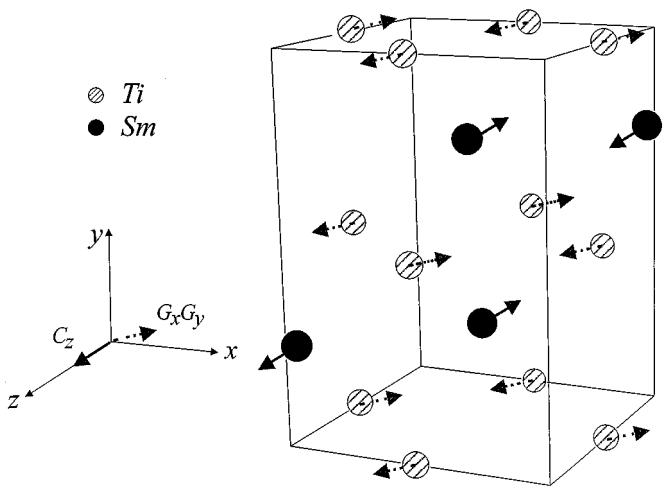

FIG. 3. Diagram showing the arrangement of spins in the *G*-type (solid arrows) and *C*-type (dashed arrows) configuration for the $x = 0$ phase.

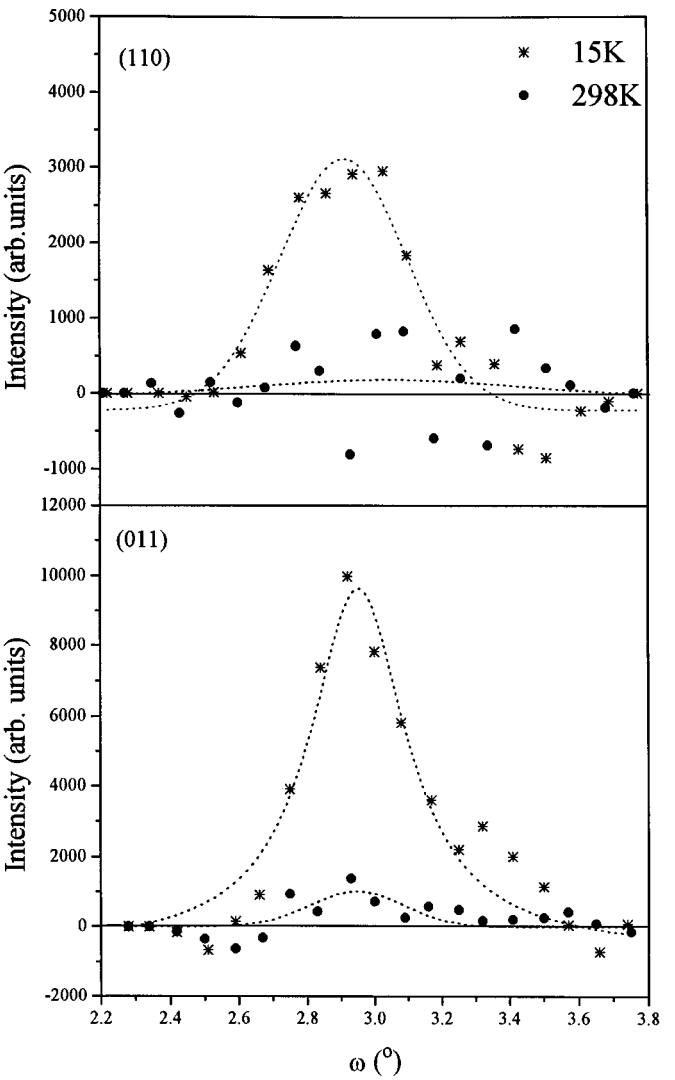

FIG. 4. Peak profiles of the *G*-type reflections (110) and (011) for the $x = 0$ phase. The dashed lines are a guide for the eyes.

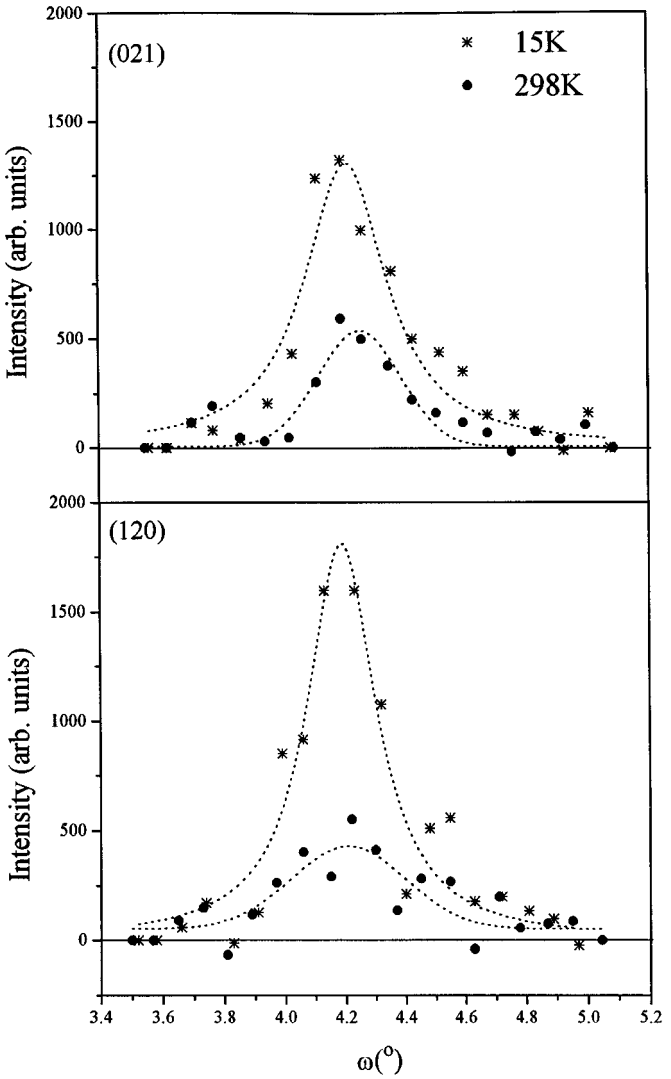

FIG. 5. Peak profiles of the *C*-type reflections (021) and (120) for the $x = 0$ phase. The dashed lines are a guide for the eyes.

are summarized in Table 6. At 298 K the presence of the (021) and (120) reflections is apparent and is likely due to multiple scattering since these reflections are forbidden in *Pnma*. The long scan times required for the observation of these magnetic peaks reflect the very small magnetic moments associated with the ordering on each sublattice.

The magnitude and orientation of the magnetic moments were determined with the program FULLPROF (16). This was done by achieving a good agreement between the observed intensities of the magnetic reflections with calculated values obtained by varying the magnitude and orientation of the moments. The scattering length of praseodymium was used for the determination due to the noninclusion of the scattering length of samarium in this program. Using the magnetic structure described above for $NdTiO_3$ as an initial model as well as several other models which placed the

TABLE 6
Integrated Intensities of the Magnetic Reflections Measured at 15 and 298 K

h	*k*	*l*	15 K	298 K
1	1	0	26(2)	0(2)
0	1	1[a]	86(2)	9(2)
0	2	1	19(1)	7(1)[b]
1	2	0	22(1)	7(1)[b]

[a] Allowed structural reflection.
[b] Due to multiple scattering.

moments along different axes, for example [Ti-(G_y); Sm-(C_z)] and [Ti-(G_z); Sm-(C_z)], we calculated the intensities of the magnetic reflections by varying the magnitude and orientation of the moments on each sublattice. To compare the calculated and observed intensities directly, the relative intensities with respect to a chosen structural peak in each case were determined. Several structural peaks were used for these comparisons and were chosen to have small 2θ values as close to the magnetic reflections as possible, as at higher values the effects of absorption and extinction are expected to become more severe. The magnitude and orientation of the magnetic moment were varied until a good agreement was found between the relative intensities in the calculated and observed cases. The best agreement was found using a model of Ti(III)-G_{xy} and Sm(III)-C_z with moments of 0.72(1) μ_B and 0.43(1) being determined for the Ti(III) and Sm(III) ions with angles of 7(3)° to the *x*-axis and 2(2)° to the *z*-axis, respectively (see Tables 7 and 8). The model is illustrated in Fig. 3. While this model appears to be consistent with Bertaut's symmetry rules (15), it must be borne in mind that there also exists a weak ferromagnetic component as evidenced by the susceptibility data. In past studies, this moment has been estimated to be very small ($\sim 10^{-2}\ \mu_B$) (6); however, nothing definitive can be stated about its magnitude and direction from the current neutron data. The value for Sm(III) compares well with that found for the Sm^{3+} ion in $SmFeO_3$ and $SmCrO_3$ at 0.45 and 0.49 μ_B, respectively (17). Hence, the results presented here show

TABLE 7
Comparison of the Calculated and Observed Relative Intensities When μ[Ti(III)] = 0.72(1) μ_B[a]

h	*k*	*l*[b]	$I_{110,calc}/I_{hkl,calc}$	$I_{110,obs}/I_{hkl,obs}$	$I_{011,calc}/I_{hkl,calc}$	$I_{011,obs}/I_{hkl,obs}$
2	0	0	0.159	0.151	0.454	0.455
0	0	2	0.058	0.057	0.166	0.17
2	1	0	6.818	6.684	19.485	20.073

[a] The moment is placed at 7(3)° from the *x*-axis.
[b] Chosen structural reflection for comparison.

TABLE 8
Comparison of the Calculated and Observed Relative Intensities When μ[Sm(III)] = 0.43(1) μ_B

h	k	l[b]	$I_{120,calc}/I_{hkl,calc}$	$I_{120,obs}/I_{hkl,obs}$	$I_{021,calc}/I_{hkl,calc}$	$I_{021,obs}/I_{hkl,obs}$
2	0	0	0.089	0.089	0.069	0.071
0	0	2	0.032	0.033	0.025	0.027
2	1	0	3.818	3.923	2.939	3.128

[a]The moment is placed at 2(2)° from the z-axis.
[b]Chosen structural reflection for comparison.

that for the first time the magnetic structure of $SmTiO_3$, and thus any other rare earth titanate, can be unequivocally determined using single-crystal neutron diffraction. The errors reported here reflect the uncertainties associated with the measured intensities, which are estimated to be less than 15%.

Finally, it should be mentioned that while magnetic ordering has been observed for $SmTiO_3$, it is found that this behavior extends, at least, to the $x = 0.05$ composition in the $Sm_{1-x}TiO_3$ family where $T_N \sim 40$ K (see Fig. 6). At the $x = 0.10$ composition, no obvious magnetic ordering is observed; however, a very subtle, broad feature is observed over ~100–250 K (see Fig. 7). While this is not fully understood at this time, it is thought to correspond to some degree of short-range magnetic order. Overall these observations parallel those observed for the $La_{1-x}TiO_3$ and the $Nd_{1-x}TiO_3$ systems, where strong electron correlation effects are present and the magnetic ordering disappears with the onset of metallic behavior for higher vacancy-doped members.

SUMMARY AND CONCLUSIONS

The results presented here, show that $SmTiO_3$ belongs to the antiferromagnetic set of rare earth titanates. The single-crystal neutron diffraction method has demonstrated unequivocally that the magnetic structure of $SmTiO_3$ consists of two canted antiferromagnetic sublattices with Ti(III)-G_xG_y and Sm(III)-C_z moment configurations. The magnetic moments were determined to be 0.72(1) and 0.43(1) μ_B for Ti(III) and Sm(III), respectively. The orientation is such that the Ti(III) moments are 7(3)° from the x-axis and the Sm(III) moments are 2(2)° from the z-axis. The magnetic behavior persists for the $Sm_{0.95}TiO_3$ composition and it is reasonable to conclude that it possesses the same magnetic structure as $SmTiO_3$ determined in this study.

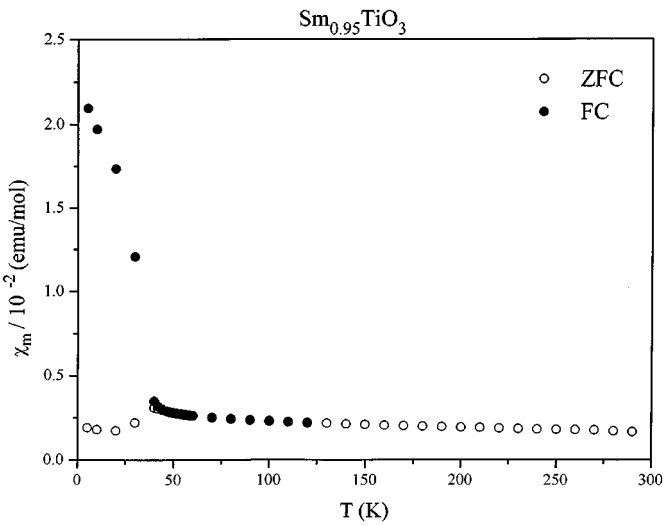

FIG. 6. Magnetic susceptibility (χ) vs T for $Sm_{0.95}TiO_3$.

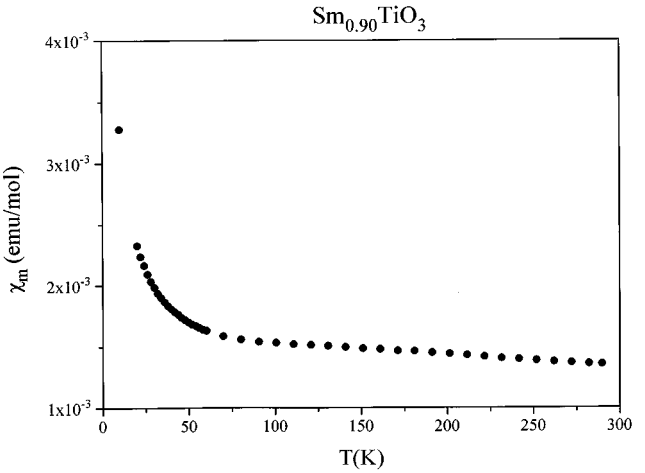

FIG. 7. Magnetic susceptibility (χ) vs T for $Sm_{0.90}TiO_3$.

ACKNOWLEDGMENTS

The authors express their gratitude to Dr. J. Britten for his contribution to this work. Financial support for this project was provided by the Canadian Institute of Neutron Scattering (CINS) and the Natural Science and Engineering Research Council (NSERC).

REFERENCES

1. M. J. MacEachern, H. Dabkowska, J. D. Garrett, G. Amow, W. Gong, G. Liu, and J. E. Greedan, *Chem. Mater.* **6,** 2092 (1994).
2. D. Crandles, T. Timusk, J. D. Garrett, and J. E. Greedan, *Phys. Rev. B* **49,** 16207 (1994).
3. C. Eylem, H. L. Ju, B. W. Eichorn, and R. L. Greene, *J. Solid State Chem.* **114,** 164 (1995).
4. Y. Fujishima, Y. Tokura, and T. Arima, *Phys. Rev. B* **46,** 11167 (1992).
5. D. A. Maclean, K. Seto, and J. E. Greedan, *J. Solid State Chemistry* **40,** 241 (1981).
6. J. P. Goral and J. E. Greedan, *J. Magn. Magn. Mater.* **37,** 315 (1983).
7. C. W. Turner and J. E. Greedan, *J. Magn. Magn. Mater.* **36,** 242 (1983).
8. G. Amow and J. E. Greedan, *J. Solid State Chemistry* **121,** 443 (1996).
9. P. Ganguly, O. Prakash, and C. N. R. Rao, *Phys. Status Solidi A* **36,** 669 (1976).
10. K. Yoshii and A. Nakamura, *J. Solid State Chem.* **133,** 584 (1997).

11. J. X. Boucherle, D. Givord, J. Laforest, and P. Morin, *in* "The Rare Earths in Modern Science and Technology" (G. J. McCarthy, J. J. Rhyne, and H. B. Silber, Eds.), Vol. 2. Plenum, New York, 1980.
12. C. Wilkinson, H. Khamis, R. F. D. Stansfield, and G. J. McIntyre, *J. Appl. Crystallogr.* **21,** 471 (1988).
13. G. M. Sheldrick, Siemens SHELXTL, Version 5.03, Siemens Crystallographic Research Systems, Madison, WI, 1994.
14. D. A. Maclean, H.-N. Ng, and J. E. Greedan, *J. Solid State Chem.* **30,** 35 (1979).
15. E. F. Bertaut, *in* "Magnetism" (G. T. Rado and H. Suhl, Eds.), Vol. III, p. 149. Academic Press, New York, 1963.
16. J. Rodriguez-Carvajal, "FULLPROF: A Program for Rietveld Refinement and Pattern Matching Analysis," Abstracts of the Satellite Meeting on Powder Diffraction of the XVth Congress of the International Union of Crystallography, p. 127, Toulouse, France, 1990.
17. M. Eibschütz, R. L. Cohen, and L. G. Van Uitert, *J. Phys. Colloq.* **32,** (Suppl. No. 2–3), C1–C922 (1971).